J. Fluid Mech. (1989), *vol.* 205, *pp.* 243–262
Printed in Great Britain

Unsteady high-Reynolds-number flows

By N. RILEY AND R. VASANTHA
School of Mathematics, University of East Anglia, Norwich NR4 7TJ, UK

(Received 2 February 1988 and in revised form 10 February 1989)

A method for calculating unsteady boundary-layer flows, based upon a vorticity–stream function formulation, has been supplemented by an appropriate viscous–inviscid interaction law to extend the calculations to large but finite Reynolds numbers. Two examples are considered in detail, namely the impulsive motion of a circular cylinder, and the flow induced when a line vortex is introduced into the neighbourhood of a circular cylinder. For the first of these a comparison of the results obtained with earlier boundary-layer and interactive calculations, Navier–Stokes solutions and experiment is made.

1. Introduction

In this paper we are concerned with unsteady viscous flows both in the high-Reynolds-number boundary-layer limit, and at high but finite values of the Reynolds number.

For steady boundary-layer flows it is well established, through the work of Goldstein (1948), that flow separation is accompanied by the appearance of a singularity at the point of vanishing skin friction. It is known that this singularity is a creature of the boundary-layer equations, and that the flow structure in the neighbourhood of separation is more complicated than that offered by boundary-layer theory if an adequate representation of the Navier–Stokes equations is to be realized. For unsteady flow in which separation, or flow breakaway, occurs the boundary-layer solution develops a singularity at a finite time. This breakdown has been demonstrated by van Dommelen & Shen (1980, 1982) in their numerical solution of the boundary-layer equations in Lagrangian coordinates for the flow past an impulsively moved circular cylinder, and the structure of the singularity at breakdown has been analysed by them. Working within an Eulerian framework both Cowley (1983), who uses series extension methods, and Ingham (1984), who uses a series truncation method, have confirmed the structure of the singularity at the point of breakdown.

Veldman (1979) has developed a practical method of calculation for steady flows at very high Reynolds numbers which retains the essence of the flow structure in the neighbourhood of separation referred to above. His method is based upon the boundary-layer equations; these are supplemented by a viscous–inviscid interaction law which incorporates the displacement effect of the boundary layer on the outer inviscid flow. His calculations of the flow past an indented plate show that the singularity at separation is removed in the interactive calculation. More recently Henkes & Veldman (1987) have adopted this interactive scheme for unsteady flows. For the impulsively moved circular cylinder they do not encounter the singular behaviour of boundary-layer theory, although the complete time-history of this particular flow cannot be achieved by a method that is based upon a thin-layer approximation.

In the present paper we have developed a method of solution of the boundary-layer equations that is based on a vorticity–stream function formulation; this is incorporated into an interactive scheme when an interaction law, in the spirit of Veldman (1979), is introduced. The advantage of our vorticity–stream function formulation is that it obviates the need to formally include any pressure variations in the boundary-layer equations. If the large normal pressure gradient, which may develop, is ignored a singularity can occur in the interactive calculations. Of course, this may be avoided by properly accounting for the normal pressure gradient as, for example, in Smith, Papageorgiou & Elliott (1984). We have applied our method to two problems both of which show breakdown at a finite time in the boundary-layer limit. In each case we have confirmed the appearance of the singularity predicted by van Dommelen & Shen. In order to achieve the accuracy required for this we have introduced grid-stretching into our procedure in the neighbourhood of the singularity.

The two problems we have addressed are (i) the impulsive motion of a circular cylinder and (ii) the flow induced when a line vortex is introduced into the neighbourhood of a circular cylinder. For (i) our boundary-layer calculations show good agreement in detail with the results obtained by others, and the results of our interactive calculations are in broad agreement with those presented by Henkes & Veldman (1987). This example provides a searching test of a high-Reynolds-number interactive method because, as the Reynolds number decreases, significant qualitative changes in the flow take place. These have been documented from careful flow visualization experiments by Bouard & Coutenceau (1980) and by Ta Phuoc Loc & Bouard (1985). The latter paper also presents numerical solutions of the Navier–Stokes equations up to Reynolds numbers $O(10^4)$, which are in good agreement with experiment. Numerical solutions up to Reynolds numbers 10^4 have also been obtained by Dennis & Staniforth (1971). For Reynolds numbers less than $O(10^4)$ the flow is relatively uncomplicated; recirculation regions develop at the rear stagnation point, as predicted by the work of Proudman & Johnson (1962), which increase in thickness and are eventually shed from the cylinder. But at higher Reynolds numbers, say $O(10^4)$, the dominant feature of the recirculation regions appears away from the rear stagnation point itself, as may be seen in figure 4 (*a*), in the form of an intense vortex which as the Reynolds number increases further becomes distinct from, but corotating with, the rear-stagnation-point eddy. It is this vortex that may be identified with the breakdown of the boundary-layer solution in the infinite-Reynolds-number limit. Our interactive calculations predict this qualitative change in the separating flow structure as the Reynolds number decreases. Moreover the value of such calculations is further emphasized by the difficulties that are experienced in the Navier–Stokes calculations for Reynolds numbers greater than 10^4, difficulties which are undoubtedly due to the complex flow structure.

In the second example of a vortex and cylinder, the breakdown of our boundary-layer calculations is in accord with the analysis of van Dommelen & Shen. This type of breakdown has also been observed by Doligalski & Walker (1984) in their study of a vortex convected along a plane boundary, and by Ersoy & Walker (1986) who consider the boundary layer on a plane boundary when a vortex pair advances to, or recedes from, it. Chuang & Conlisk (1989) have carried out interactive calculations for the convected vortex, and although their calculations proceed beyond the boundary-layer breakdown point the solution does eventually fail, possibly for the reasons indicated above. We have experienced no breakdown in our interactive calculations although, as with (i), no steady-state solution is available, and our

results cannot be extended to the point where vortex shedding from the cylinder takes place. The flow structure at large finite Reynolds number is seen to be dominated by the appearance of a single eddy close to the cylinder, and slightly ahead of the vortex, as predicted by the boundary-layer calculations.

2. The governing equations

The Navier–Stokes equations of motion for an incompressible fluid of density ρ and kinematic viscosity ν may be written as

$$\frac{\partial \bar{\boldsymbol{v}}}{\partial \bar{t}} - \bar{\boldsymbol{v}} \wedge \bar{\boldsymbol{\omega}} = -\nabla(\bar{p}/\rho + \tfrac{1}{2}\bar{v}^2) - \nu \nabla \wedge \bar{\boldsymbol{\omega}}, \quad \nabla \cdot \bar{\boldsymbol{v}} = 0. \tag{1a, b}$$

In these equations $\bar{p}$ is the pressure, $\bar{\boldsymbol{v}}$ the velocity, and $\bar{\boldsymbol{\omega}} = \nabla \wedge \bar{\boldsymbol{v}}$ the vorticity. If the pressure is eliminated by taking the curl of (1 *a*) we recover Helmholtz's equation for the vorticity $\bar{\boldsymbol{\omega}}$. Our interest in this paper is with two-dimensional flows that are bounded internally by a circular cylinder, for which polar coordinates $(\bar{r}, \theta)$ are appropriate. If the corresponding velocity components are $(\bar{v}, \bar{u})$ then (1 *b*) is satisfied identically if we introduce a stream function $\bar{\psi}$ such that

$$\bar{v} = \frac{1}{\bar{r}} \frac{\partial \bar{\psi}}{\partial \theta}, \quad \bar{u} = -\frac{\partial \bar{\psi}}{\partial \bar{r}}. \tag{2}$$

The vorticity $\bar{\boldsymbol{\omega}} = (0, 0, \bar{\omega})$ for this two-dimensional situation, where

$$\bar{\omega} = \frac{1}{\bar{r}} \left\{ \frac{\partial}{\partial \bar{r}} (\bar{r}\bar{u}) - \frac{\partial \bar{v}}{\partial \theta} \right\} = -\nabla^2 \bar{\psi}, \tag{3}$$

and ∇^2 is the two-dimensional Laplacian. The equation satisfied by $\bar{\omega}$ is, from Helmholtz's equation,

$$\frac{\partial \bar{\omega}}{\partial \bar{t}} + \frac{\bar{u}}{\bar{r}} \frac{\partial \bar{\omega}}{\partial \theta} + \bar{v} \frac{\partial \bar{\omega}}{\partial \bar{r}} = \nu \nabla^2 \bar{\omega}. \tag{4}$$

In (3) and (4) we now introduce dimensionless variables and, simultaneously, the classical boundary-layer scaling. We take the cylinder radius a as a typical length, and a/U_r as a time, where U_r is some reference velocity. If we then write

$$\bar{r} = a(1 + \epsilon y), \quad \bar{\psi} = \epsilon U_r a \psi, \quad \bar{u} = U_r u, \quad \bar{v} = \epsilon U_r v, \quad \bar{\omega} = \frac{U_r}{a\epsilon} \omega, \tag{5}$$

where $Re = \epsilon^{-2} = U_r a/\nu$ is the Reynolds number, (3) and (4) may be written as

$$\omega = -\frac{\partial^2 \psi}{\partial y^2}, \quad \frac{\partial \omega}{\partial t} + u \frac{\partial \omega}{\partial \theta} + v \frac{\partial \omega}{\partial y} = \frac{\partial^2 \omega}{\partial y^2}. \tag{6a, b}$$

In deriving (6*a*, *b*) terms which are formally $O(\epsilon)$, due to the curvature of the boundary surface, have been omitted.

The boundary conditions require, in addition to an initial condition at $t = 0$, that $\psi = 0$ on $y = 0$, $\partial\psi/\partial y \to -u_s$ where u_s is the inviscid slip velocity, and $\omega \to 0$ as $y \to \infty$. We further require a condition on ω at the boundary which we derive, in §3, from the no-slip condition $u = 0$ at $y = 0$, and finally that ω and ψ are periodic in θ with period 2π.

Now, in this paper we are not only interested in solutions of the unsteady boundary-layer equations, and their breakdown at a finite time heralding flow-

separation, but also in solutions at large but finite Reynolds numbers. To find such solutions we adopt a viscous/inviscid interaction technique, and we anticipate that singularities which are a creature of the boundary-layer equations will be suppressed. In that respect our solutions, still based upon a thin-layer approximation, are in accord with the Navier–Stokes solutions. The interactive constructions which inhibit the appearance of a singularity are local multistructured constructions centred upon the point at which the boundary-layer solution develops a singularity. Veldman (1979) and Henkes & Veldman (1987), see also references cited therein, have pointed out the obvious difficulty of incorporating a local solution of this type into a composite solution. They indicate the desirability of working with a composite equation. Such an equation is (6), provided that the interaction between the thin viscous layer and the outer inviscid flow is properly treated. It is the viscous displacement velocity $v_\infty = \mathrm{d}(u_\mathrm{s}\delta)/\mathrm{d}\theta$, where

$$\delta = \int_0^\infty (1-u/u_\mathrm{s})\,\mathrm{d}y$$

is the displacement thickness, which drives the perturbation to the outer potential flow. When this is incorporated into the outer inviscid solution it results in a slip velocity on the cylinder surface $y = 0$ given by

$$u_\mathrm{s}(\theta,t) = u_\mathrm{sp}(\theta,t) - \frac{\epsilon}{2\pi}\int_0^{2\pi} \frac{\mathrm{d}(u_\mathrm{s}\delta)/\mathrm{d}\theta \sin(\alpha-\theta)}{1-\cos(\alpha-\theta)}\,\mathrm{d}\alpha. \tag{7}$$

In (7) $u_\mathrm{sp}(\theta,t)$ is the slip velocity at $y = 0$ predicted by potential theory, and the integral is a Cauchy principal value integral.

In arriving at (6) we have formally assumed, in (5), that $\bar{v} = O(\epsilon)$, and so is comparable with curvature effects. Within the interaction region $\bar{v}$ will be much larger than is implied by (5), and this will be made manifest by larger numerical values of v in the solutions obtained for small but finite values of ϵ. A consequence of this is that it is an entirely consistent procedure to neglect curvature terms in (6) and only retain the effects of finite Reynolds number, or non-zero ϵ, in (7). In his treatment of the displacement velocity, Veldman (1979) evaluates the integral in (7) only over the region of strong interaction. This again is consistent with the idea that $v_\infty \gg 1$ there, but remains $O(1)$ elsewhere.

The stream function–vorticity formulation of the problem we are proposing in (6) is commonly used in the solution of the Navier–Stokes equations, but its use with the boundary-layer equations is less common. An obvious disadvantage of the formulation is that the boundary vorticity is not prescribed *a priori*. However, the advantage to be gained is that the pressure is eliminated from the problem, and therefore so is the need to consider any pressure perturbations in the interactive calculations. If the flow develops such that $\partial v/\partial\theta = O(\epsilon^{-2})$ then the approximation (6*a*) to (3) fails and the solution may, once again, terminate in a singularity. Such an event has not taken place in our calculations, where the thin-layer approximation has proved to be the limiting factor†.

† *Note added in proof.* It should, however, be noted that Smith (1988) has demonstrated that breakdown at a finite time can occur in any unsteady interacting boundary layer.

3. Numerical procedures

Each of the flows which we consider in §4 below is initiated by an impulsive motion. In the initial stages of the flow development interactive effects are unimportant and the solution of (6) is the Rayleigh solution

$$\left.\begin{aligned} \omega &= \frac{u_{\mathrm{sp}}}{(\pi t)^{\frac{1}{2}}} \mathrm{e}^{-\frac{1}{4}\eta^2} + O(t^{\frac{1}{2}}), \\ \psi &= -u_{\mathrm{sp}} \int_0^{\eta} \mathrm{erf}\,(\tfrac{1}{2}s)\,\mathrm{d}s + O(t), \quad \eta = y/t^{\frac{1}{2}}. \end{aligned}\right\} \tag{8}$$

We have taken (8) as our starting solution, evaluated at $t = 0.01$, for both our boundary-layer and interactive studies. To advance the solution beyond this initial time we have used a finite-difference scheme which we now describe.

Consider the evaluation of (6) for ω and ψ, in finite-difference form, at the point $i\delta\theta$, $j\delta y$, $k\delta t$, where $\delta\theta$, δy, δt are the step lengths adopted for θ, y and t respectively in the calculation. We have used central differences throughout to represent derivatives with respect to t and y. As we advance the solution in θ, and our technique involves making successive sweeps from $\theta = 0$ to 2π, we must ensure that regions of reversed flow can be satisfactorily handled. If $u_{i,j,k} > 0$ then the representation of the θ-derivative in (6*b*) as $(\omega_{i,j,k} - \omega_{i-1,j,k})/\delta\theta$ leads to a stable procedure. However, if $u_{i,j,k} < 0$ we must represent that derivative as $(\omega_{i+1,j,k} - \omega_{i,j,k})/\delta\theta$ to maintain stability. In the latter case this requires information about ω ahead of the point at which the solution is being sought. In our iterative procedure such information would be available from the previous sweep or, during the first sweep, from the solution at the previous time level. Upwind differencing of this type leads to a stable iterative procedure but only maintains an accuracy $O(\delta\theta)$. In the boundary-layer calculations accuracy in θ is at a premium as breakdown is approached, as we shall see below. This being so we have adopted as a representation of the θ-derivative, the form $(\omega_{i+1,j,k} - \omega_{i-1,j,k})/2\delta\theta$. This leads to accuracy $O(\delta\theta^2)$, and at the same time does not involve $u_{i,j,k}$, and therefore its sign, in the estimation of $\omega_{i,j,k}$. This has worked well in our boundary-layer calculations, but has lead to instabilities in our interactive calculations, for which we have adopted the upwind difference formulation. The matrix of coefficients of the finite-difference equations which results from the discretization described above is of tridiagonal form; the equations are solved by a standard algorithm.

To update the solution at each station $i\delta\theta$ it is necessary to know, or have some estimate, of $\omega_{i,0,k}$, namely the value of ω at $y = 0$. We evaluate this quantity as follows. The no-slip condition requires $u_{i,0,k} = 0$. We calculate $u_{i,j,k}$, $j = 1$ to 4 from ψ, using a difference formula accurate to $O(\delta y)^4$; and from $\omega_{i,0,k} = \partial u/\partial y|_{y=0}$ we use a five-point one-sided formula to express $\omega_{i,0,k}$ in terms of $u_{i,j,k}$, $j = 1$ to 4.

As we have mentioned above, in the boundary-layer calculations resolution of the flow details with respect to the coordinate θ is at a premium at the point in the boundary layer where breakdown occurs, say $\theta = \theta_{\mathrm{s}}$. To enhance the resolution in the neighbourhood of $\theta = \theta_{\mathrm{s}}$ we have introduced grid stretching into our boundary-layer calculations. Thus for flows that are symmetrical about $\theta = 0$, as for example the impulsively moved circular cylinder, with breakdown at $\theta = \pm\theta_s$, we have introduced a new angular coordinate α with

$$\frac{\mathrm{d}\theta}{\mathrm{d}\alpha} = \left\{1 + \frac{\cos 2\alpha_{\mathrm{s}}}{2(1+\lambda)^2}\right\}^{-1} \left\{1 - \frac{\cos(\alpha - \alpha_{\mathrm{s}})}{1+\lambda}\right\} \left\{1 - \frac{\cos(\alpha + \alpha_{\mathrm{s}})}{1+\lambda}\right\}. \tag{9}$$

In (9) λ is a parameter which has taken the value 0.1 in our calculations, and $\alpha = \alpha_s$ is the point which corresponds to $\theta = \theta_s$. The singular point θ_s is not known *a priori* in any particular problem, but may be estimated from a preliminary calculation in which there is no grid stretching. When only one such singular point is present, as for our example of a line vortex in the presence of a circular cylinder, we adopt for our grid stretching

$$\frac{\mathrm{d}\theta}{\mathrm{d}\alpha} = 1 - \frac{\cos(\alpha - \alpha_s)}{1+\lambda}, \tag{10}$$

where we have taken $\lambda = 0.4$ in our calculations. We have only used the grid stretching, represented by (9) and (10), for our boundary-layer calculations. For the interactive calculations the high resolution offered by this device has not proved to be necessary.

Our iterative method, in advancing the solution from t to $t+\delta t$, proceeds in the following steps. (i) With the values of u, v in (6*b*) taken as at time t, equations (6) are integrated by sweeping from $\theta = 0$ to 2π, with one pass across the viscous layer at each station to update ω and ψ. (ii) If the periodicity condition is not satisfied step (i) is repeated. In practice we find that a second sweep is only necessary for the asymmetric vortex and cylinder problem. (iii) The value of $\omega_{i,0,k}$ is updated, and the earlier steps repeated until this quantity is satisfactorily converged. For the impulsively moved cylinder this quantity has to be updated more than one hundred times in the boundary-layer calculation as the breakdown time is approached, but never more than twenty in the interactive calculation. By contrast, for the vortex and cylinder problem fewer than seven such changes are required in either the boundary-layer or interactive calculations. (iv) At this point (u, v) are updated from ψ, and the foregoing steps repeated. For the impulsively moved cylinder up to fifty changes in (u, v) may be required to satisfy a convergence criterion in the boundary-layer calculations as breakdown is approached, whilst only three or four such updates are required for the vortex and cylinder problem. For our interactive calculations these are replaced by thirty and ten respectively. For the boundary-layer calculation we now have a converged solution at time $t+\delta t$. For the interactive calculations a further step (v) is required in which $u_s(\theta, t)$ in (7) is changed. This is achieved by estimating the derivative of $\int_0^\infty (u_s - u)\,\mathrm{d}y$, using central differences, with the current estimate of u_s. In the subsequent evaluation of the integral in (7) the singular part is subtracted before using Simpson's rule in the numerical evaluation. In practice, where there is significant interaction we have found that for the impulsively moved cylinder as many as six updates of u_s (with only half that number for the vortex and cylinder problem) may be required before we proceed to the next time level.

The method described above works well in practice. It is not swift in operation, but then we have made no especial effort to improve its efficiency. In §4 below we apply the method to two problems; first the impulsively moved circular cylinder, and second the flow induced when a line vortex is suddenly introduced to the neighbourhood of a circular cylinder.

4. Examples

4.1. *The impulsively moved cylinder*

We apply the method outlined in §3 above to the flow around a circular cylinder which is impulsively set into motion at time $t = 0$ with speed U_0. We take our reference velocity $U_r = 2U_0$ so that $u_{sp} = \sin\theta$.

Several authors have addressed this problem and a useful reference source is the

paper by Henkes & Veldman (1987). In particular one notes the seminal papers of van Dommelen & Shen (1980, 1982). These authors have not only obtained accurate solutions of the boundary-layer equations in a Lagrangian framework but have also uncovered the structure of the singularity which occurs in the solution at $t = t_s$, beyond which no solution exists. They estimate $t_s = 3 \pm 0.05$ (1980), $t_s = 3.0045$ (1982). The latter is probably the most accurate estimate that is available. They also find $\theta_s = 111°$. Several authors present results from calculations carried out within the Eulerian framework. From these we mention in particular the work of Cowley (1983), Ingham (1984), Cebeci (1986) and Henkes & Veldman (1987). Cowley's approach is to extend the Blasius time-series expansion, which he does by up to as many as 51 terms, and then recast the series using rational functions. In this way he is able to calculate important flow properties up to about $t = 2.8$. His estimate of the breakdown time is $t_s = 3.00$. Ingham uses a method of series truncation in which the vorticity and stream function are expanded as sine-series whose coefficients satisfy ordinary differential equations which are integrated numerically. He uses up to 180 terms in the truncated series from which he can estimate flow properties up to $t = 2.94$. His results suggest $t_s = 3.00$. Henkes & Veldman employ a finite-difference method for both the boundary-layer equations *per se*, and the interaction equations. For the boundary-layer equations they encounter a stability problem in their calculations at about $t = 2.8$. But this is almost certainly a grid-size problem and only serves again to emphasize the high accuracy that is required to resolve the details of the solution close to the singular point. Their results are otherwise in good agreement with those of Cowley and Ingham.

In our calculations, the results of which we now present, we have taken the outer edge of the computational domain to be at $y_\infty = 25$ with $\delta y = 0.25$. Although the increment in y may be thought to be rather coarse, numerical experimentation shows that it is entirely adequate. It is the step sizes δt and $\delta\theta$ that must be small if the flow details are to be resolved close to the singular point. We have chosen $\delta t = 0.01$.

For $\delta\theta$ various experiments have been done. We can report that with $\delta\theta = \pi/360$ without any grid stretching, the results are much less accurate than when we take $\delta\alpha = \pi/180$, with grid stretching as in equation (9). The results from our calculations are presented in figures 1–3 where shear stress, displacement thickness and the viscous displacement velocity are presented, respectively. The shear stress is perfectly well-behaved up to the breakdown point, as has been noted by other authors. The displacement thickness gives some hint of the difficulties that are to be encountered as $t \to t_s$. At first, see figure 2, the dominant feature is the rapid increase in displacement thickness at the rear stagnation point. The work of Proudman & Johnson (1962) shows that $\delta|_\pi \to \infty$ as $t \to \infty$. However there is already evidence at $t = 2.9$ of the event that terminates the solution at the finite time $t = t_s$. But, as Cowley (1983) has observed, it is the viscous displacement velocity v_∞ that might be expected to reveal in a dramatic fashion the presence of a singularity in the solution. That this is so may be seen in figure 3. These results may be compared with Cebeci (1986, figure 5). There, no hint of singular behaviour for $t \approx 3.0$ is observed, which leads him to conjecture that the only singularity is that associated with the steady-state solution. This view is not shared by the present, or other, authors and casts doubt over the effectiveness of the method of solution proposed by Cebeci. The work of van Dommelen & Shen (1980) shows that as $t \to t_s$, $v_\infty \sim C(t_s - t)^{-\frac{1}{4}}$, where C is a constant. Further, as we see from figure 3, the angular region over which the rapid rise in v_∞ takes place diminishes in extent as $t \to t_s$. If $\Delta\theta_s$ is a measure of this it can be shown that $\Delta\theta_s = O\{(t_s - t)^{\frac{3}{4}}\}$. This latter result demonstrates the need for high

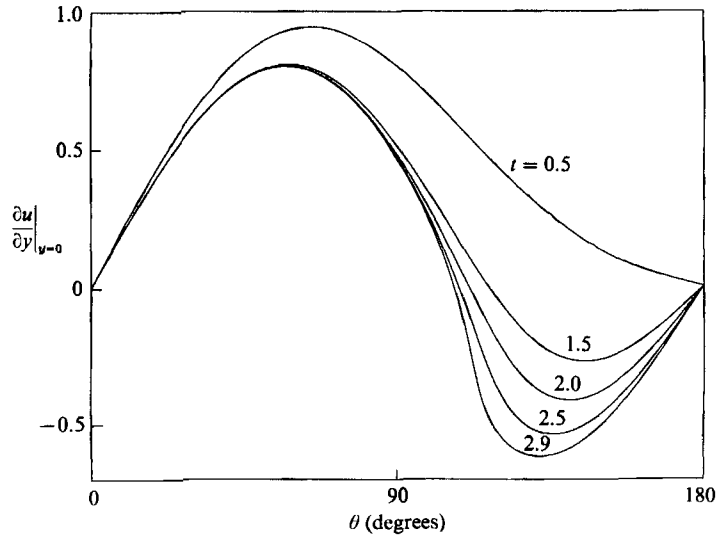

FIGURE 1. The skin friction, at various values of t, from the boundary-layer calculation.

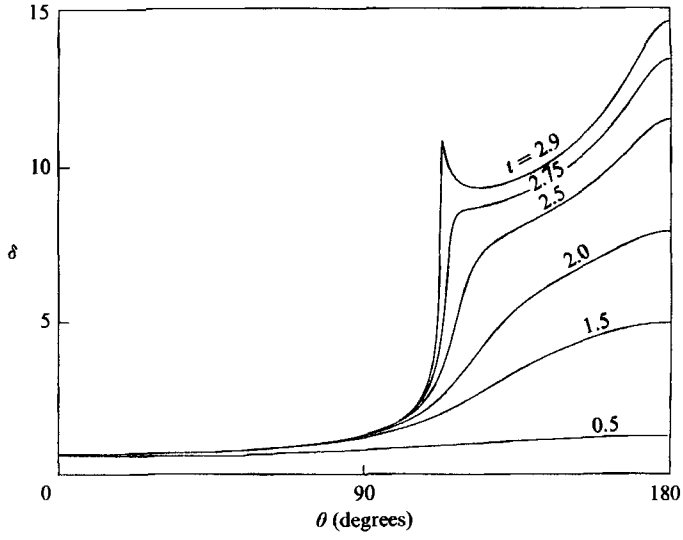

FIGURE 2. The displacement thickness δ, at various values of t, from the boundary-layer calculation.

resolution close to $\theta = \theta_s$ as $t \to t_s$. We have extended our solution to $t = 2.94$ and for $t \geqslant 2.7$ we have shown that a plot of $\log v_\infty$ versus $\log(t_s - t)$ yields a straight line of slope $-\frac{7}{4}$, in accord with the analysis of the singularity by van Dommelen & Shen, with $t_s = 3.01$.

We believe that the foregoing shows that the numerical method we have described in §3 is more effective and accurate than other finite-difference methods applied to this problem. The situation to which we have applied it above provides a particularly severe test, if only because through not taking advantage of the obvious symmetry we have, for $\theta > \pi$, been integrating *ab initio* against the main flow direction.

We turn next to the interactive calculation that we have carried out for this case.

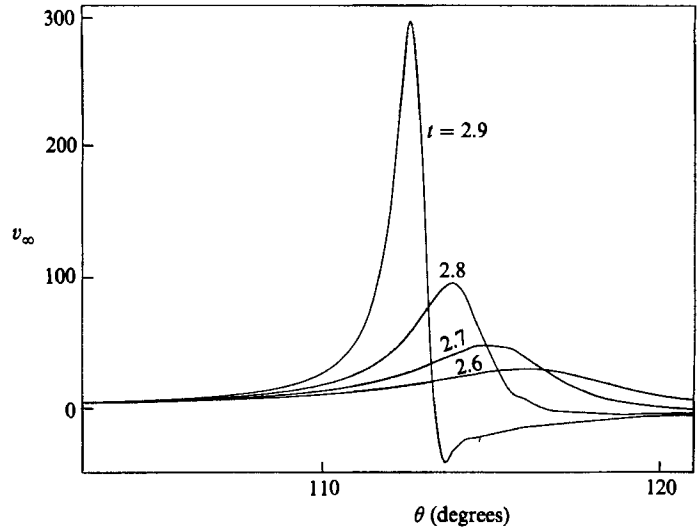

FIGURE 3. The viscous displacement velocity v_∞, at various values of t, from the boundary-layer calculation.

Previous results have been presented by Henkes & Veldman (1987) for Reynolds numbers 10^4, 10^5 and 10^6 corresponding to $\epsilon = 10^{-2}$, 3.16×10^{-3}, 10^{-3} respectively. As we have already indicated we have not found it necessary to introduce grid stretching into these calculations. The reason for this is that in the interaction region, where breakaway of the flow is taking place, we no longer have the singular behaviour experienced with the boundary-layer equations. At finite Reynolds number the interaction region extends, according to Elliot, Smith & Cowley (1983), over an angular distance $O(\epsilon^{\frac{3}{22}})$. Our calculations with $\delta\theta = \pi/90$ appear to adequately resolve the interaction. We have again set $y_\infty = 25$ and taken $\delta y = 0.25$, $\delta t = 0.01$.

Before we present any results from our interactive calculations we draw attention to experimental features of these flows, as observed from the striking flow visualizations of Bouard & Coutenceau (1980) and Ta Phuoc Loc & Bouard (1985). In figure 4(*a*), reproduced from Ta Phuoc Loc & Bouard, we see the flow over the rear part of a circular cylinder at $t = 4$, for $Re = 9500$, following an impulsive start. The dominant feature for $\frac{3}{4}\pi < \theta \leqslant \pi$ is a large recirculating eddy, E say, ahead of which another small feature is seen to be developing. The eddy E consists (see figure 4*b*), essentially, of two parts. In the neighbourhood of the rear stagnation point the recirculating flow is in a relatively thin region, say R, whilst ahead of it is a more prominent feature, which we refer to as the primary eddy P. The part R is a manifestation of the 'lift-off' of the boundary layer at the rear stagnation point as described by Proudman & Johnson (1962). At the earlier time $t = 2$ the parts P and R of E are not distinguishable. As t increases P develops rapidly to subsume R until at $t = 6$ there is to be seen a pair of standing eddies, symmetrically disposed about $\theta = \pi$, prior to vortex shedding. As the Reynolds number decreases P becomes a less prominent feature. Thus at $Re = 3000$, we see from the experimental results of the Poitiers group presented by Ta Phuoc Loc & Bouard (1985) that, in E, P no longer dominates as the eddy expands to form the vortex pair prior to shedding. The experimental features at these two Reynolds numbers have been confirmed from numerical solutions of the Navier–Stokes equations, obtained by Ta Phuoc Loc & Bouard (1985). Numerical solutions, in broad agreement with these, have also been

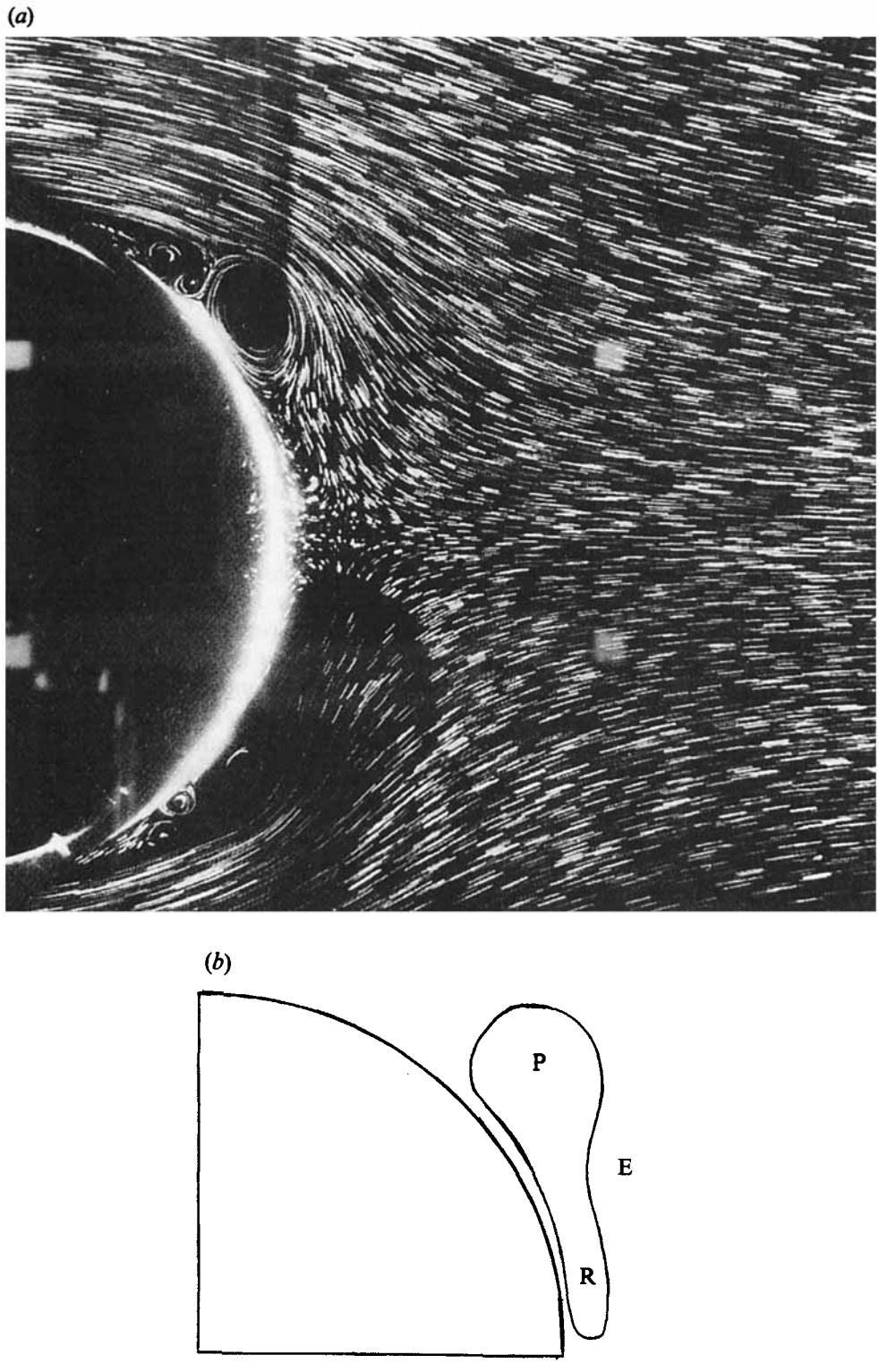

FIGURE 4(*a*). The flow pattern over the rear part of the cylinder at $t = 4$, from Ta Phuoc Loc & Bouard (1985), (*b*) explanatory sketch.

obtained by Dennis & Staniforth (1971). As Re increases above $O(10^4)$ we might expect the part P of the eddy E to become even more vigorous, and indeed the interactive calculations of Henkes & Veldman (1987) show that at $Re = 10^5$ the parts P and R split into individual corotating eddies at $t = 3$. It is not surprising, therefore, that S. C. R. Dennis (private communication) reports extreme difficulty in obtaining Navier–Stokes solutions for Re in excess of 10^4. The qualitative changes, described above, in the flow development over the rear part of the cylinder, as we move up through the Reynolds-number range, is a feature of our interactive calculations which we now present.

We have chosen to base the discussion of our results upon the viscous displacement velocity v_∞ shown in figure 5 and the shear stress $\partial u/\partial y|_{y=0}$ shown in figure 6, from which the important flow properties may be inferred. Consider first the displacement velocity. There is no evidence of the singular behaviour at $t \approx 3$ which is shown to be developing in the boundary-layer calculation (figure 3). In fact, in all cases the extrema are reduced. However beyond $t = 3$ new features emerge. Consider figure 5(*b*) for the case $Re = 10^5$. For $t > 3.2$ there is, in addition to the large positive and negative peaks in v_∞, an additional region in which v_∞ is positive. The distribution of v_∞ for $t > 3$ is entirely consistent with a flow development, beyond separation, of two corotating eddies, as described by Henkes & Veldman (1987), and alluded to above. We turn next to the case $Re = 10^4$ shown in figure 5(*c*). The flow development is now dominated by that of the rear-stagnation-point eddy, referred to above as R, with no apparent 'individualization' of what we have described above as the primary eddy P. This qualitative change in the behaviour of the flow is in accord with that noted above in our discussion of the experimental results. We cannot, of course, expect our calculations to describe the situation much beyond the point to which we have taken them. Our interactive equations (6) and (7) are based upon a thin-layer approximation, and it is well-known that the developments we are describing beyond separation do not long remain within a thin layer. Figure 4(*a*) bears witness to this.

For very high Reynolds number we would expect, at least for times up to which the boundary-layer calculation fails, that the interactive calculation will yield results that are close to those of boundary-layer theory and that the two calculations will diverge, at a given time, as the Reynolds number decreases. This is clearly seen in figure 5, but the differences are even more striking when we consider the shear stress distributions in figure 6. The most noticeable feature, which is confirmed from results obtained at intermediate Reynolds numbers, is that the minimum of the shear stress does not vary monotonically with Re at a given time. However, as with figure 5(*c*), the results of figure 6 again show the qualitative change that takes place in the flow properties as the Reynolds number decreases and the individualization of a primary eddy does not occur. It seems unlikely that an interactive calculation of the present type can be wholly successful in describing a flow whose dominant features do not reflect those of the high-Reynolds-number limit. That our results are open to question at Reynolds numbers $O(10^4)$ and less is suggested from a comparison with the accurate Navier–Stokes calculations of Dennis & Staniforth (1971). Our results are seen, in figure 6, to differ from those of Dennis & Staniforth. They are very similar to the results of Henkes & Veldman (1987) at $Re = 10^4$, although somewhat closer to the Navier–Stokes predictions. Henkes & Veldman suggest that the discrepancy may be due to finite curvature effects. However, we have carried out calculations in which the terms $O(\epsilon)$ in our governing equations are included, and report a *negligible* change in the results at $Re = 10^4$. We are forced to conclude that there is a Reynolds number below which interactive theories of the type used here, and elsewhere, are of

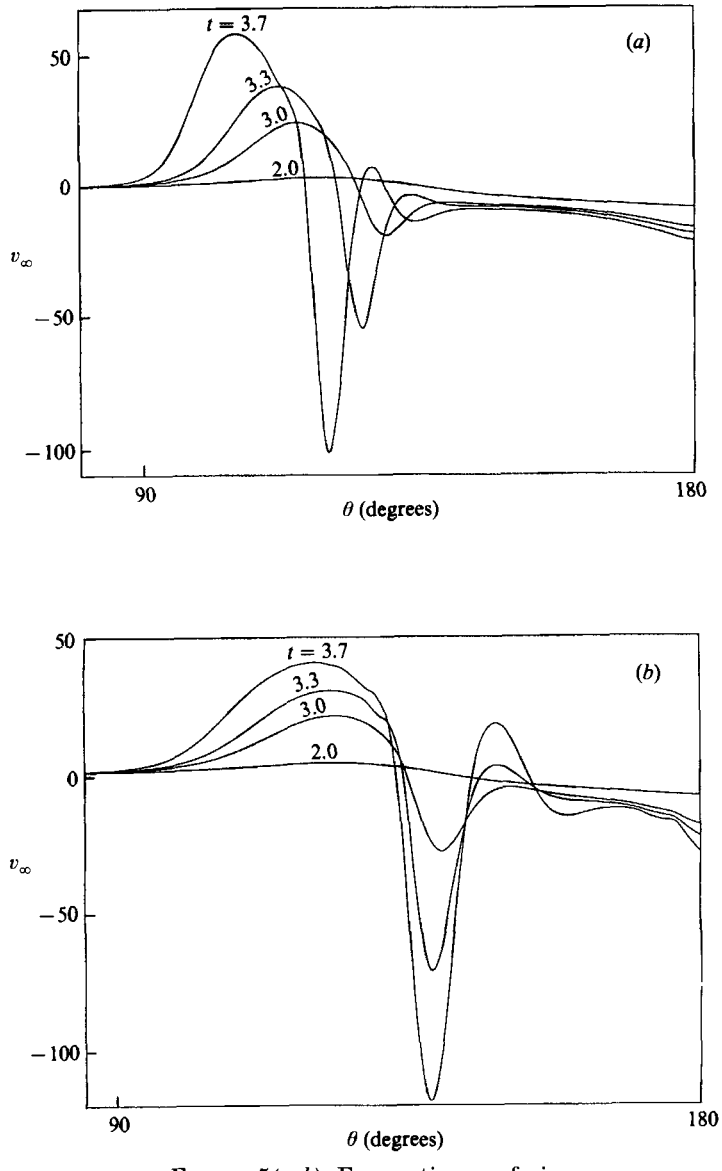

FIGURE 5(*a*, *b*). For caption see facing page.

limited value in relation to the Navier–Stokes equations for unsteady complex flows, except at small values of time. At the same time we again comment on the apparent difficulty in obtaining solutions of the Navier–Stokes equations for this problem for Reynolds numbers in excess of 10^4, and suggest that this is not entirely unconnected with the vigorous viscous–inviscid interaction which we have demonstrated in figures 5 and 6.

4.2. *The vortex and cylinder*

In this section we apply the method outlined in §3 to determine the flow that is induced when an inviscid line vortex with circulation Γ is introduced, at time $t = 0$,

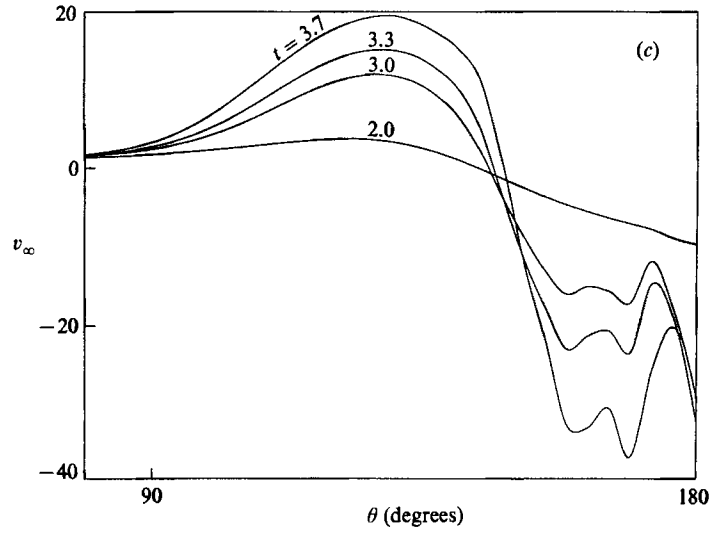

FIGURE 5. The viscous displacement velocity v_∞, at various values of t, from the interactive calculation. (*a*) $Re = 10^6$, (*b*) 10^5, (*c*) 10^4.

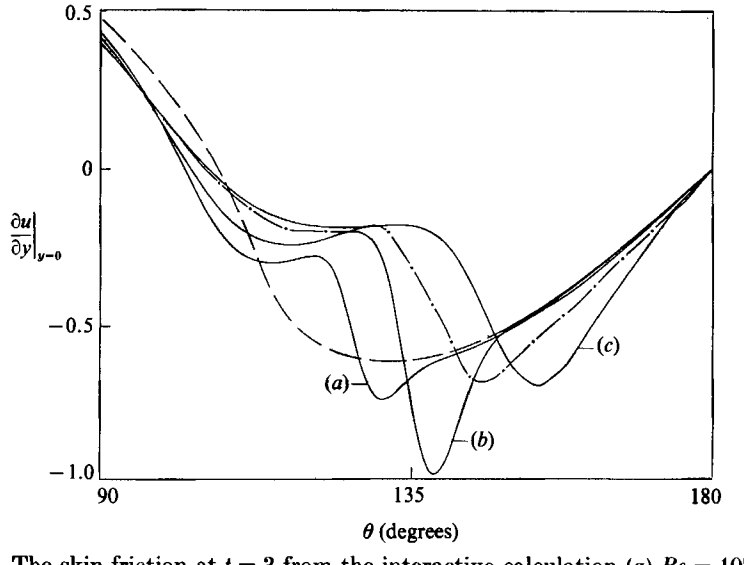

FIGURE 6. The skin friction at $t = 3$ from the interactive calculation (*a*) $Re = 10^6$, (*b*) 10^5, (*c*) 10^4: –·–·–, at $t = 3$, $Re = 10^4$ from the Navier–Stokes equations (Dennis & Staniforth 1979); ––––, at $t = 2.94$ from the boundary-layer calculation.

in the vicinity of, and parallel to, a circular cylinder. We take the reference velocity $U_r = \Gamma/\nu$, and if the vortex is initially at the point (R, π) then

$$\left.\begin{aligned} u_{sp} &= \frac{1}{2\pi}\left\{1 - \frac{R^2-1}{R^2+1-2R\cos(\theta-\Theta)}\right\}, \\ \text{where} \quad \Theta &= \pi - \frac{t}{2\pi R^2(R^2-1)}. \end{aligned}\right\} \tag{11}$$

Figure 7 provides a definition sketch of this situation.

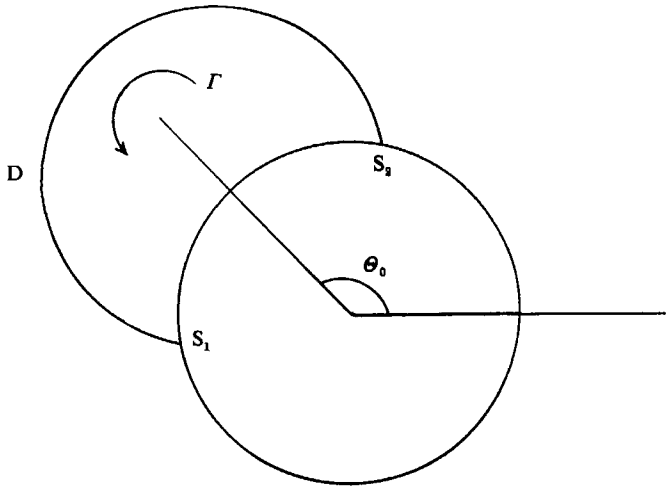

FIGURE 7. Definition sketch. S_1, S_2 represent the stagnation points of attachment and separation respectively, D is the dividing streamline and θ_0 the initial angular position of the vortex.

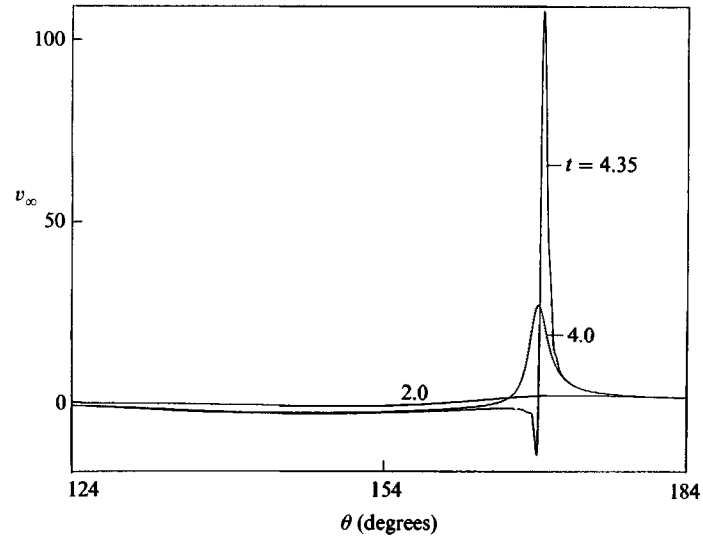

FIGURE 8. The viscous displacement velocity v_∞, at various values of t, from the boundary-layer calculation.

As with the previous example we first consider the limiting case of boundary-layer flow. Our calculations have been carried out with the numerical parameters set as for the previous example, namely $y_\infty = 25$, $\delta y = 0.25$, $\delta t = 0.01$, $\delta\alpha = \pi/180$, with grid stretching implemented as represented by equation (10). We again present our results, obtained for $R = 2$, in the form of the viscous displacement velocity v_∞, figure 8, and the boundary shear stress $\partial u/\partial y|_{y=0}$, figure 9. The dominant, and expected, feature is the development of a singularity in our solution at a finite time. This is again to be seen most clearly in the behaviour of the displacement velocity in figure 8. A careful examination of our results shows that the singular behaviour is as predicted by van Dommelen & Shen (1980) with the breakdown time $t_s = 4.64$. During this time the vortex has moved an angular distance of only $3\frac{1}{2}°$. This rapid

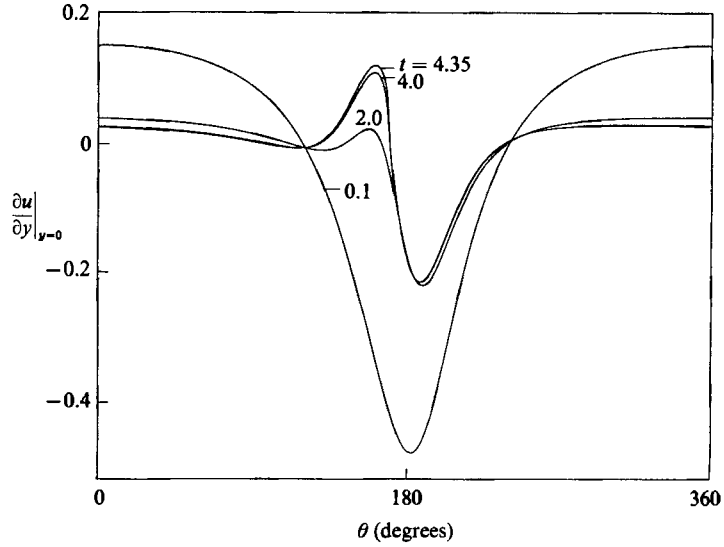

FIGURE 9. The skin friction, at various values of t, from the boundary-layer calculation.

breakdown of the boundary-layer solution, witnessed also in §4.1, is typical of these unsteady boundary-layer situations, and has also been encountered by Doligalski & Walker (1984) in their study of a rectilinear vortex convected past a plane boundary, and by Ersoy & Walker (1986) who consider the motion of a vortex pair over a plane boundary. The flow details before this breakdown of the solution occurs may be inferred from figures 8 and 9. At the initial instant there are stagnation points of attachment and separation on the boundary at $\theta = \frac{4}{3}\pi$ and $\frac{2}{3}\pi$ respectively. Throughout the period of the flow development up to breakdown these points move only slightly, following the direction of motion of the vortex. At about $t = 1$ significant changes in the flow between the angular position of the vortex and the stagnation point of separation ahead of it, begin to take place. A flow reversal, as indicated by the region of positive shear stress which develops and by the distribution of v_∞, indicates a growing eddy ahead of, and in which the vorticity has opposite sign to, the driving vortex. This is as to be expected in the adverse pressure gradient ahead of the vortex, exactly as for the impulsively moved cylinder. This flow development ends abruptly at $t = t_s$ in the boundary-layer calculation.

We have carried out calculations for different values of R, but note no qualitative changes in the flow development described above. The breakdown time t_s increases monotonically with R, although the angular distance moved by the vortex during this time changes little.

The interactive calculations have been carried out in the manner described in §4.1 for the impulsively moved cylinder. We have again employed the upwind-difference scheme, and used the same computational mesh. Consistent with our neglect of the terms $O(\epsilon)$ in (6) we have ignored any viscous diffusion of the vortex. However, we have incorporated into our scheme the effect of displacement on the vortex position, though in practice this is negligible. The vortex position (R, Θ) is determined as follows. If (V, U) are the radial and transverse components of velocity at the vortex then we have

$$R = R_0 + \int_0^t V \, dt, \quad \Theta = \Theta_0 + \int_o^t \frac{U}{R} dt, \tag{12}$$

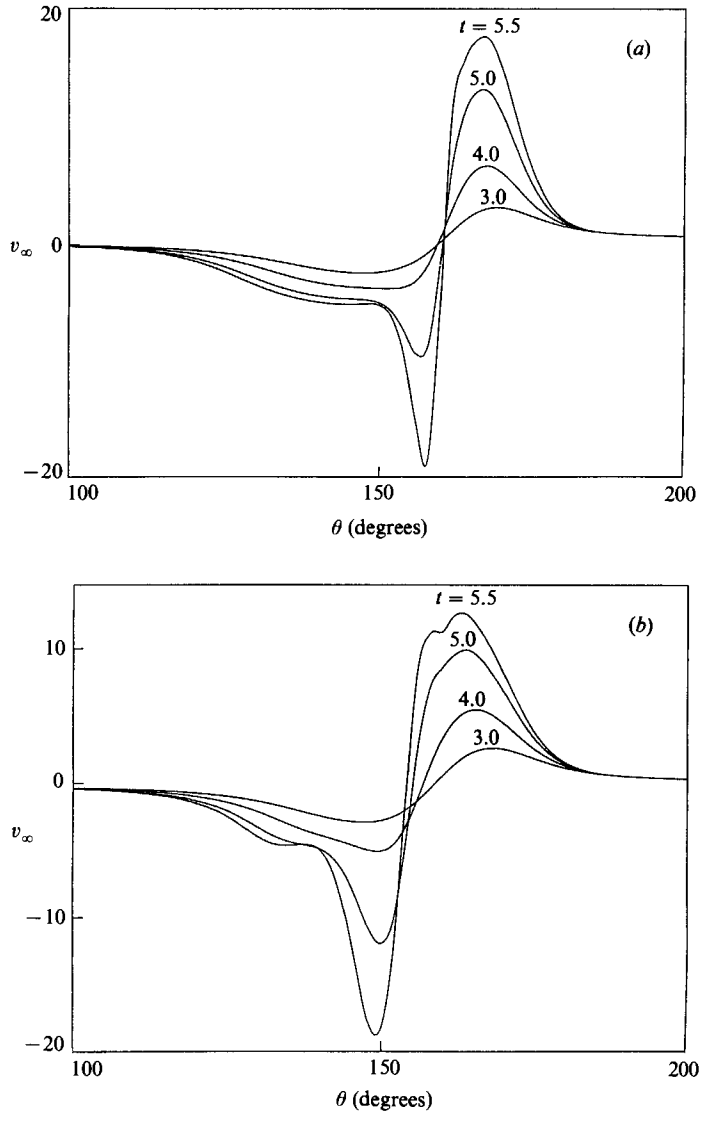

FIGURE 10. The viscous displacement velocity v_∞, at various values of t, from the interactive calculation. (*a*) $Re = 10^6$, (*b*) 10^5.

where

$$\left.\begin{aligned} U &= -\frac{1}{2\pi R(R^2-1)} - \frac{\epsilon}{\pi}\int_0^{2\pi} \frac{v_\infty \sin(\mu-\Theta)\,\mathrm{d}\mu}{1+R^2-2R\cos(\mu-\Theta)}, \\ V &= -\frac{\epsilon}{\pi}\int_0^{2\pi} \frac{\{R-\cos(\mu-\Theta)\}\,\mathrm{d}\mu}{1+R^2-2R\cos(\mu-\Theta)}, \end{aligned}\right\} \tag{13}$$

with (R_0, Θ_0), the initial vortex position, equal to $(2, \pi)$ in our calculations.

We again centre our discussion of the results we have obtained on the viscous displacement velocity and the shear stress at the cylinder. But before we consider these in detail we remark that this flow is a much less complex flow than that which we considered in §4.1. In that flow we noted the qualitative changes that take place

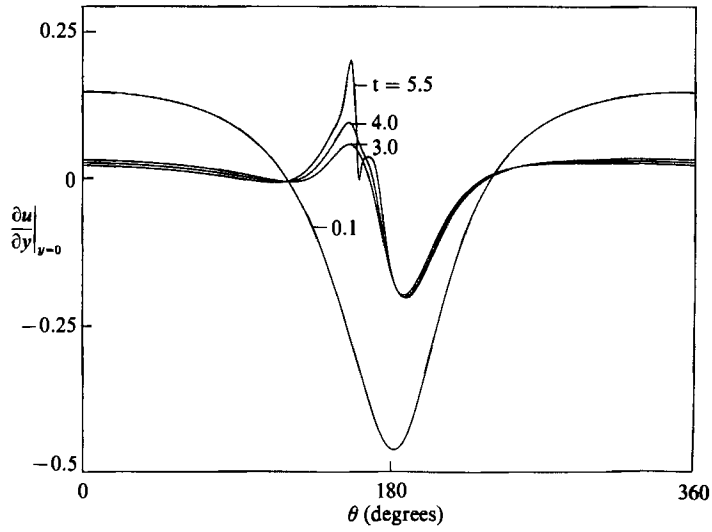

FIGURE 11. The skin friction, at various values of t, from the interactive calculation. $Re = 10^6$.

as the Reynolds number decreases, with the primary eddy P becoming less prominent whilst the recirculation region R at the rear stagnation point assumes a more significant role. There is no such feature associated with the vortex-induced flow over the cylinder and as a consequence our calculations, again carried out at $Re = 10^6$, 10^5 and 10^4, show no qualitative differences, and indeed reflect the features that we have already noted in our discussion of the boundary-layer solution.

The viscous displacement velocity is shown in figure 10, with the shear stress in figure 11. Since there are no qualitative changes to be observed we have included results only at $Re = 10^6$ and 10^5. We have, as expected, been able to continue our integration of (6) beyond the singular point of the boundary-layer solution. However, as in the previous example there is no steady-state solution to be achieved here, and we can only expect our interactive calculation to be valid as long as the thin-layer approximation upon which it is based remains valid. The most noticeable feature of our results is, again, a reduction in the peak of the displacement velocity, shown in figure 10. This maximum is located just ahead of the vortex, which itself has moved an angular distance of only about 4° at $t = 5.5$; beyond that is a region of comparably large negative velocity. This distribution of the viscous displacement velocity, taken together with that of the skin friction shown in figure 11, clearly demonstrates the existence of an eddy, arising from flow separation, just ahead of the vortex. The flow development described above is clearly seen in the streamline patterns shown in figure 12. These streamline patterns complement those presented by Henkes & Veldman (1987) for the flow past an impulsively moved cylinder. Like those authors we have stretched the radial scale outside the cylinder, in this case by a factor ϵ^{-1}, in order to reveal the flow details. Thus the separated flow region is very thin, and occupies no more than about 8% of the cylinder radius. As the flow develops further, beyond the scope of our interactive calculation, this situation must change dramatically as vortex shedding from the cylinder takes place.

An interactive calculation has also been carried out, in the Eulerian framework, for a rectilinear vortex convected past a plane boundary in a uniform flow by Chuang & Conlisk (1989). Although the solution is continued beyond the time at which the

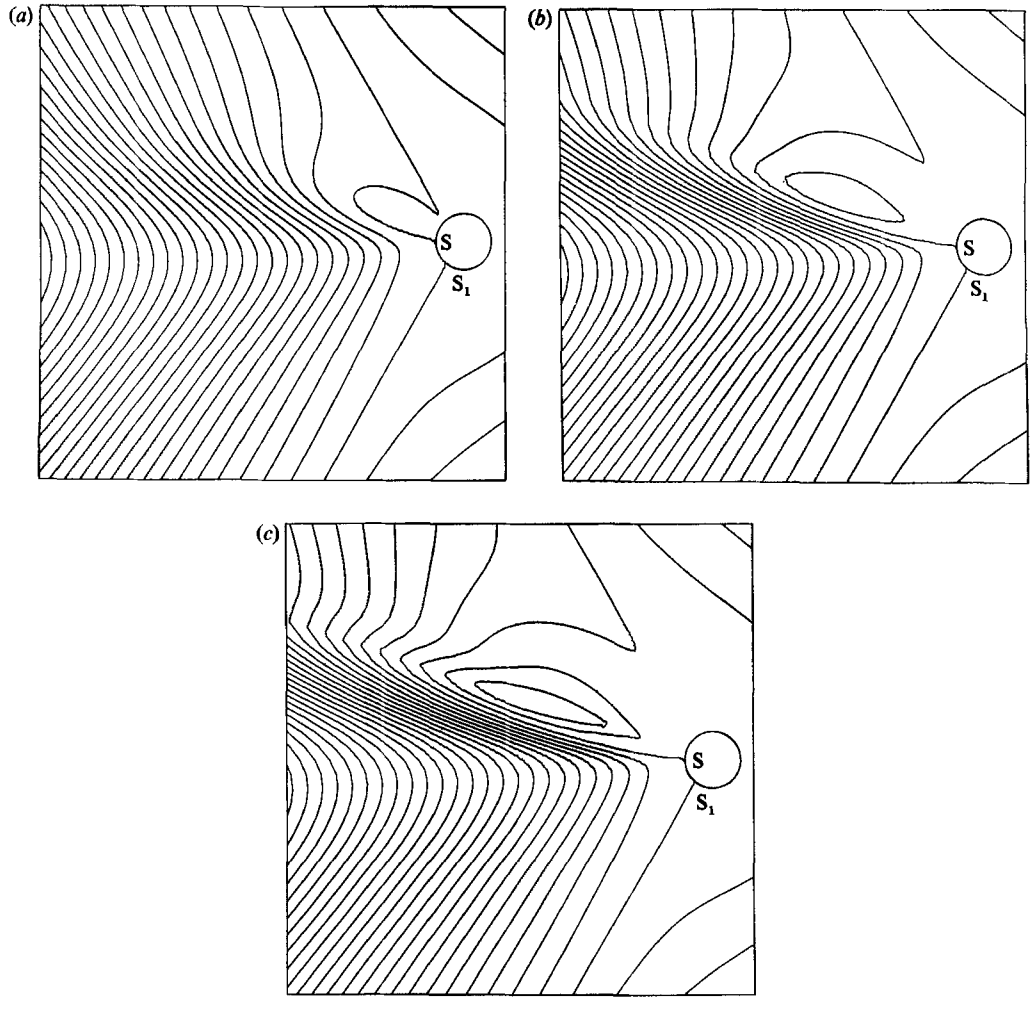

FIGURE 12. Streamlines from the interactive calculation for $Re = 10^6$ at (*a*) $t = 3$, (*b*) 4.5, (*c*) 5. S_1 is the stagnation point of attachment, S the point of flow separation. The scale for $r > 1$ has been magnified by a factor ϵ^{-1}.

boundary-layer calculation fails, it breaks down as the strong interaction develops. We attribute our success, in this respect, to the use of the stream function–vorticity formulation in which no assumptions about the pressure gradient are required.

5. Conclusions

In this paper we have developed a method of calculation for unsteady high-Reynolds-number flows, which includes the limiting boundary-layer case. Boundary-layer calculations have been carried out for the impulsive flow past a circular cylinder, and the flow induced when a line vortex is introduced into the neighbourhood of a circular cylinder. These calculations terminate in a singular behaviour at a finite time, with a structure that is in accord with the analysis of van Dommelen & Shen (1980). The solutions have been extended to high, but finite, values of the Reynolds number using a viscous–inviscid interaction model which is

based upon a thin-layer approximation. Calculations carried out using this model indicate that the boundary-layer singularity is removed. No singularity has appeared in our interactive calculations. However, in neither of the problems we have considered is a steady-state solution available, and our procedures can only be valid as long as the thin-layer approximation itself remains valid. The results we have obtained for the impulsively moved cylinder confirm the results obtained by Henkes & Veldman (1987), and recover, qualitatively anyway, features of the careful observations made of this flow by Bouard & Coutenceau (1980). With confidence established in the effectiveness of our interactive method we have used it to reveal the initial, developing, flow features when a line vortex is introduced to the neighbourhood of a circular cylinder. We have shown how a recirculating separated flow region develops ahead of the vortex but, restricted as we are to cases in which the eddy must remain thin, we are not able to continue the calculation up to the point where shedding of vorticity from the cylinder surface takes place.

The authors gratefully acknowledge valuable discussions with M. Coutenceau, S. J. Cowley, S. C. R. Dennis, L. L. van Dommelen and F. T. Smith. R.V. was supported by an SERC Visiting Fellowship during the period in which this work was carried out.

REFERENCES

BOUARD, R. & COUTENCEAU, M. 1980 The early stage of development of the wake behind an impulsively started cylinder for $40 < Re < 10^4$. *J. Fluid Mech.* **101**, 583–608.

CEBECI, T. 1986 Unsteady boundary layers with an intelligent numerical scheme. *J. Fluid Mech.* **163**, 129–140.

CHUANG, F. S. & CONLISK, A. T. 1988 The effect of interaction on the boundary layer induced by a convected rectilinear vortex. *J. Fluid Mech.* **200**, 337–365.

COWLEY, S. J. 1983 Computer extension and analytic continuation of Blasius expansion for impulsive flow past a circular cylinder. *J. Fluid Mech.* **135**, 389–405.

DENNIS, S. C. R. & STANIFORTH, A. N. 1971 A numerical method for calculating the initial flow past a cylinder in a viscous fluid. In *Proc. 2nd Intl Conf. Num. Meth. Fluid Dyn.* Lecture Notes in Physics, Vol. 8, pp. 343–349. Springer.

DOLIGALSKI, T. L. & WALKER, J. D. A. 1984 The boundary layer induced by a convected two-dimensional vortex. *J. Fluid Mech.* **139**, 1–28.

DOMMELEN, L. L. VAN & SHEN, S. F. 1980 The spontaneous generation of the singularity in a separating laminar boundary layer. *J. Comput. Phys.* **38**, 125–140.

DOMMELEN, L. L. VAN & SHEN, S. F. 1982 The genesis of separation. In *Numerical and Physical Aspects of Aerodynamic Flows* (ed. T. Cebeci), pp. 293–311. Springer.

ELLIOTT, J. W., SMITH, F. T. & COWLEY, S. J. 1983 Breakdown of boundary layers: (i) On moving surfaces; (ii) in semi-similar unsteady flow; (iii) in fully unsteady flow. *Geophys. Astrophys. Fluid Dyn.* **25**, 77–138.

ERSOY, S. & WALKER, J. D. A. 1986 Flow induced at a wall by a vortex pair. *AIAA J.* **24**, 1597–1605.

GOLDSTEIN, S. 1948 On laminar boundary layer flow near a point of separation. *Q. J. Mech. Appl. Maths.* **1**, 43–69.

HENKES, R. A. W. M. & VELDMAN, A. E. P. 1987 On the breakdown of the steady and unsteady interacting boundary-layer description. *J. Fluid Mech.* **179**, 513–529.

INGHAM, D. B. 1984 Unsteady separation. *J. Comput. Phys.* **53**, 90–99.

PROUDMAN, I. A. & JOHNSON, K. 1962 Boundary layer growth near a rear stagnation point. *J. Fluid Mech.* **12**, 161–168.

SMITH, F. T., PAPAGEORGIOU, D. & ELLIOTT, J. W. 1984 An alternative approach to linear and nonlinear stability calculations at finite Reynolds number. *J. Fluid Mech.* **146**, 313–330.

SMITH, F. T. 1988 Finite-time break-up can occur in any unsteady interacting boundary layer. *Mathematika* **35**, 256–273.

TA PHUOC LOC & BOUARD, R. 1985 Numerical solution of the early stage of the unsteady viscous flow around a circular cylinder: a comparison with experimental visualization and measurements. *J. Fluid Mech.* **160**, 93–117.

VELDMAN, A. E. P. 1979 A numerical method for the calculation of laminar incompressible boundary layers with strong viscous–inviscid interaction. *NLR TR* 79023*U*.